

Phases and critical transport of the $SU(N)$ Hofstadter-Hubbard model on the triangular lattice

Lu Zhang, Rongning Liu, and Xue-Yang Song*

Department of Physics, Hong Kong University of Science and Technology, Clear Water Bay, Hong Kong, China

(Dated: March 13, 2025)

We study phases and transitions of a triangular Hubbard model subject to commensurate magnetic field, called the Hofstadter-Hubbard model. At filling one fermion per site, for the number of fermion flavors $2 \leq N \leq 4$, we identify three distinct phases and calculate critical interaction strength from self-consistent mean-field approximation. Integer quantum Hall, chiral spin liquid, and valence bond solid (or stripe) states could be realized upon varying the Hubbard interaction U . We study the critical transport behavior using quantum Boltzmann equations for general N for the putative continuous transition from quantum Hall states to chiral spin liquid. The critical behavior serves as strong signatures of the critical theory and consequently of the existence of chiral spin liquid as the proximate phase.

Introduction—Quantum spin liquid (QSL) has been proposed as the parent state of high-temperature superconductors[1, 2]. It refers to highly entangled ground states for quantum magnets with emergent gauge structure and fractional excitations. The search for quantum spin liquids and the transition into proximate phases have been a central topic in condensed matter physics. Among various spin models, the antiferromagnetic Heisenberg model on the triangular lattice has been suggested to host the spin liquid phase due to magnetic frustration[1]. However, it has now been shown that the ordered magnetic phase is more stable than the proposed spin liquid phase[3, 4].

Among various spin liquid states, chiral spin liquid(CSL) refers to a spin liquid state with non-vanishing spin chirality[5].It is a gapped phase and has been a search target for decades, given its proposed relationship to anyon superconductivity[5, 6]. In this work, we systematically study the Hofstadter-Hubbard model on the triangular lattice(See Fig. 1(a)) for N flavors of fermions, with $SU(N)$ symmetry in the flavor space. The fermions are subject to both onsite Hubbard interaction U and commensurate magnetic field from orbital coupling. In contrast to the Hubbard model, there exists a finite flux threading through each triangle incorporating explicitly time-reversal breaking. In the large- U limit this flux results in a chirality term $\mathbf{S}_i \cdot (\mathbf{S}_j \times \mathbf{S}_k)$ in addition to the nearest neighbor Heisenberg interaction. At $N = 2$, CSL and a critical transition to integer quantum Hall states at half filling has been found numerically and proposed to result in anyon superconductivity upon doping[7, 8].

Here we study the case for general $2 \leq N \leq 8$ by means of self-consistent calculations in the salve particle formalism. In the intermediate coupling regime our analysis demonstrates that the system enters CSL phase more readily in the presence of non-trivial flux than the $SU(N)$ Hubbard model. In the weak coupling regimes, the system exhibits the integer quantum Hall(IQH) phase, as the absence of a Fermi surface precludes potential instabilities. The phase boundary between the IQH and CSL

from our mean-field calculations, aligns well with the numerical results at $N = 2$ [7]. For strong coupling, the mean field calculation reports valence bond solid(VBS) or stripe phases for $2 \leq N \leq 4$.

In addition to the topological phases in different coupling regimes, this model also serves as an excellent platform to study the quantum criticality from IQH to CSL, which is proposed as scalar QED_3 coupled with a Chern-Simons term[8], with the level determined by N . As an interacting theory, proposed to be conformally invariant[9], the transport properties are characterized by a set of universal quantities. We employ the quantum Boltzmann equation to study the finite temperature electrical conductivity, applicable to the hydrodynamic regime, where $\hbar\omega \ll k_B T$ [10]. We discuss thermodynamic properties and electrical conductivities close to the critical point at finite temperatures, as a hallmark of the critical theory. In particular the longitudinal conductivity jumps to finite value at the critical point.

This model is not only of conceptual importance but also experimentally accessible. When $N = 2$, the model can be realized in moiré bilayers in the magnetic field by treating the layer degrees of freedom as the pseudo-spin[11]. The more general $SU(N)$ model can also be modeled in an optical lattice with synthetic gauge field[12–15]. The definitive experimental signature of the spin liquid remains elusive. However, in these experimental platforms simulating the Hofstadter-Hubbard model, our proposed conductivity jump serves as a strong transport signature of the IQH-CSL transition. The critical behavior heralds the long-sought CSL phase in experiments.

CSL in $SU(N)$ Hofstadter-Hubbard model—The setup consists of the $SU(N)$ Hofstadter-Hubbard model on the triangular lattice shown in Fig. 1(a). The Hamiltonian reads

$$H = -t \sum_{\langle ij \rangle} \left(e^{iA_{ij}} c_{i\alpha}^\dagger c_{j\alpha} + \text{H.c.} \right) + \frac{U}{2} \sum_{i, \alpha \neq \beta} n_{i\alpha} n_{i\beta}, \quad (1)$$

where $\alpha = 1, \dots, N$ is the flavor indices and A_{ij} is the

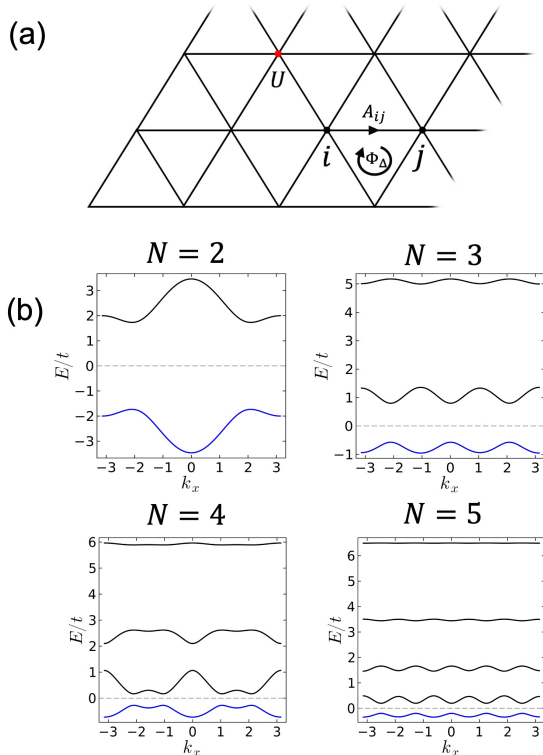


FIG. 1. (a) The triangular lattice with gauge A_{ij} defined on the bond. The flux Φ_{Δ} piercing each triangle is π/N . The electrons feel an on-site Hubbard interaction U . (b) The single particle band structure of $SU(N)$ Hofstadter-Hubbard model along the line $(k_x, 0)$. The lowest band is filled by tuning the chemical potential

external electromagnetic gauge field. The flux of each triangular plaquette is $\Phi_{\Delta} = \pi/N$, with an enlarged N -site unit cell. In the absence of the Hubbard interaction, the single particle spectrum of $SU(N)$ Hofstadter model is shown in Fig. 1(b). We consider the case where only the lowest band is filled (highlighted in blue), which corresponds to filling one fermion per site. Since there are N flavors of electrons, the band is N -fold degenerate.

Upon considering Hubbard interaction, the model incorporates strong correlation and topology, however impermeable to exact solutions. We resort to parton formalism and mean field to study the model. Recently, there are several pieces of numerical works[7, 8, 11, 16, 17] on the $SU(2)$ Hofstadter model on the triangular lattice, proposing various magnetic and topological phases. Our model is naturally the $SU(N)$ generalization of the model.

Strong Coupling Regime—To determine the phase in the strong coupling limit, we first apply the perturbation theory to reduce the Hubbard model to the Heisenberg

model. To the third order, the Hamiltonian is given by

$$H = J_2 \sum_{\langle ij \rangle} S_i^{\alpha\beta} S_j^{\beta\alpha} + J_3 \sum_{ijk \in \Delta} \exp(-i\Phi_{\Delta}) S_i^{\alpha\beta} S_j^{\beta\gamma} S_k^{\gamma\alpha}, \quad (2)$$

where $S_i^{\alpha\beta}$ is the $SU(N)$ generators and the Einstein summation is adopted. We decompose the generators $S_i^{\alpha\beta}$ in terms of the spinon creation and annihilation operators $S_i^{\alpha\beta} = f_{i\alpha}^{\dagger} f_{i\beta}$. In the parton formalism, the Hilbert space is enlarged. Therefore, the constraint $\sum_{\alpha} f_{i\alpha}^{\dagger} f_{i\alpha} = 1$ must be imposed to project the enlarged Hilbert space back to the original space. We note that there is a study[18] that examines the Hofstadter Hubbard model on the square lattice using the slave rotor approach. In our study of the strong coupling regime, we go an order further in perturbation theory and adopt a spinon formalism to improve the methodology.

Using perturbation theory, we find the parameters $J_2 = \frac{2t^2}{U}$ and $J_3 = \frac{6t^3}{U^2}$ (see Appendix for detailed derivation). To obtain the correct large- N limit we rescale the couplings $\tilde{J}_2 = NJ_2$ and $\tilde{J}_3 = N^2J_3$ to be fixed as N is changing. The saddle point can now be determined by the following mean-field Hamiltonian and its associated self-consistency equation[19]:

$$H = \sum_{\langle ij \rangle} \chi_{ij} f_{i\alpha}^{\dagger} f_{j\alpha} - \sum_i \mu_i f_{i\alpha}^{\dagger} f_{i\alpha}, \quad (3)$$

where the auxiliary field $\chi_{ij} = \sum_{\langle ij \rangle} -\frac{\tilde{J}_2}{N} \langle f_{j\alpha}^{\dagger} f_{i\alpha} \rangle + \frac{\tilde{J}_3}{N^2} \sum_{k \in \Delta_{ij}} e^{-i\Phi_{\Delta_{ij}}} \langle f_{j\alpha}^{\dagger} f_{k\alpha} \rangle \langle f_{k\alpha}^{\dagger} f_{i\alpha} \rangle$. In the self-consistency process, we select an enlarged unit cell $m \times n$ ($m, n > N$) to capture the VBS translational symmetry breaking phase. The gauge constraint can only be satisfied on average by adjusting the chemical potential to ensure that each site is occupied by only one spinon, such that $\langle f_{i\alpha}^{\dagger} f_{i\alpha} \rangle = 1$. We begin with a random initial ansatz and converge to a local minimum, in terms of the free energy. Our calculations indicate that the ground state is CSL phase characterized by average π/N flux per triangle in the hopping χ_{ij} for $N = 2, \dots, 8$ at intermediate U/t . The hopping flux corresponds to the spin chirality in the physical systems. The spinons hence fill N Chern bands with total Chern number $C_f = N$, corresponding to $U(1)_N$ CSL. The results are presented in Fig. 2.

When the Hubbard interaction U is small (less than the critical point U_{c1}), the system is in the $\nu = N$ IQH phase, as expected from the free electron limit $U = 0$. Since the IQH phase is a gapped phase without a Fermi surface, there is no instability in the weak coupling regime. As U exceeds the critical point U_{c1} , it is shown that the ground state transitions to the CSL phase.

When $N < 5$ the system undergoes a phase transition from the CSL to the VBS as U increases. The following provides an intuition to understand this result. Without magnetic field, ($\Phi_{\Delta} = 0$), the ground state of the $SU(N)$ Hubbard model breaks translation when $N < 5$ [20]. The

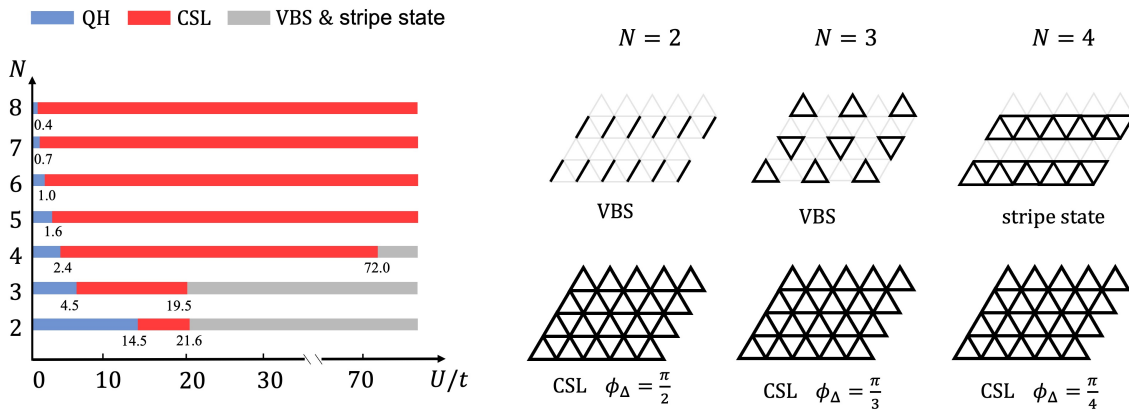


FIG. 2. Left: phase diagram of the Hofstadter-Hubbard model of coupling strength U/t and the N . It is calculated using the slave rotor mean field in the weak coupling limit and spinon parton in the strong coupling limit. Right: the schematic representation of the ansatz $\chi_{ij} = \langle f_i^\dagger f_j \rangle$ of chiral spin liquid(CSL) states, valence bond solid(VBS) and stripe state as a function of N . The thickness of the link schematically represents the magnitude of χ_{ij} .

CSL is the closest competing state. In our model, the external magnetic field introduces the chirality term $\mathbf{S} \cdot (\mathbf{S} \times \mathbf{S})$, which energetically favors the CSL phase. The strength of this chirality term is $J_3 \sim \frac{1}{U^2}$. As U increases, the system remains in the CSL phase until it reaches the second critical point, U_{c_2} . At this point, the effect of the chirality term is insufficient to maintain the system in the CSL phase. The transition from CSL to VBS is a cross of energy of CSL versus VBS at mean-field level. It is unclear whether the transition could be a continuous transition accounting for gauge fluctuations, and this remains to be studied in the future.

The CSL phase tends to exist in a wider range of interaction strength as one increases N , intuitively understood from the point that frustration increases as N increases. An anomaly is that the U_{c_2} slightly decreases for $N = 3$, compared to $N = 2$. This may be due to the geometry of triangular lattice: a commensurate 3 – site unit cell VBS where the electrons form an SU(3) singlet, naturally exists for SU(3) model (shown in Fig. 2). Hence VBS is favored in SU(3) case.

While when $N = 5$ the ground state of the Hubbard model is the stripe state and the energy difference between the CSL (lowest competing state) and the ground state is small such that the chirality term always leads to the CSL phase (In our mean-field calculation, we find that there is no translation symmetry-breaking phase with lower energy than spin liquid). For $N > 5$, the CSL is the lowest energy state due to the frustration of the SU(N) model [20, 21], with or without chirality terms.

Intermediate Coupling Regime—In the intermediate coupling regime, the system undergoes a transition between the IQH and CSL phases. In the free fermion limit $U = 0$, the system hosts a simple non-interacting ground state, which corresponds to the IQH phase. As the parameter U increases, the system becomes more localized

and transitions into the CSL phase. We employ the slave rotor approach to determine the critical point. By introducing the rotor variable $e^{i\theta}$ and its conjugate angular momentum $L_i = i\partial_{\theta_i}$ on each site, we express the annihilation operator as $c_{i,\sigma} = f_{i,\sigma} e^{i\theta_i}$. The fermion operator is decomposed into a combination of spinon operator f_σ and rotor $e^{i\theta}$, thus separating the effect of the magnetic flux. This rewriting introduces a gauge redundancy: a $U(1)$ phase rotation on $f_i \rightarrow f_i e^{i\varphi}$, $e^{i\theta_i} \rightarrow e^{i\theta_i} e^{-i\varphi}$ leaves the physical fermions invariant. Later to go beyond mean-field, we couple the theory to a $U(1)$ gauge field a . The gauge redundancy is removed by imposing a constraint at each site, $L_i + \sum_\sigma f_{i,\sigma}^\dagger f_{i,\sigma} = 1$, where we adopt the convention that the rotor quantum number $L_i = 0$ corresponds to $\frac{1}{N}$ -filling. The Hubbard Hamiltonian (1) in terms of the spinon and rotor can be rewritten as

$$H = - \sum_{\langle ij \rangle, \sigma} t e^{iA_{ij}} e^{-i(\theta_i - \theta_j)} f_{i,\sigma}^\dagger f_{j,\sigma} + \text{h.c.} + \frac{U}{2} \sum_i L_i^2. \quad (4)$$

To make further progress, we perform the mean-field decomposition of the above Hamiltonian:

$$\begin{aligned} H_{\text{MF}} &= H_f + H_\theta, \\ H_f &= -\tilde{t} \sum_{\langle ij \rangle, \sigma} e^{iA_{ij}} f_{i,\sigma}^\dagger f_{j,\sigma} + \text{h.c.}, \\ H_\theta &= -J \sum_{\langle ij \rangle, \sigma} \psi_i^\dagger \psi_j + \text{h.c.} + \frac{U}{2} \sum_i L_i^2. \end{aligned} \quad (5)$$

Here we have replaced the rotor variable $e^{i\theta}$ with a uni-modular field ψ_i . \tilde{t} and J are the mean-field parameters: $\tilde{t} \equiv \frac{1}{zN_s} \sum_{\langle ij \rangle} t \langle \psi_i^\dagger \psi_j \rangle + \text{h.c.}$, and $J \equiv \frac{1}{zN_s} \sum_{\langle ij \rangle, \sigma} t e^{iA_{ij}} \langle f_{i,\sigma}^\dagger f_{j,\sigma} \rangle + \text{h.c.}$. N_s is the total site number and $z = 6$ is the coordination number. The magnetic field is explicitly assigned to the spinon sector

in Eq.(5). This is verified by the mean field solution detailed in appendix : the spinons f_σ hop in the same flux as the physical magnetic field, while the rotors ψ feel vanishing flux. Hence the N species of spinons stay in Chern bands with total Chern number $C_f = N$.

The phase transition is determined by the behavior of the rotor, governed by a Hubbard Hamiltonian Eq.(5) and displays a superfluid-Mott transition. In the superfluid state, the rotor condenses, fermions are identified as spinons and fill N Chern bands, forming the IQH state. Conversely, in the Mott state, the rotors are gapped, leading to the CSL. Solving H_f, H_θ self-consistently(see Appendix), we arrive at the critical interaction U_{c_1} (shown in Fig. 2). When $N = 2$, the critical point $U_{c_1}/t \approx 14.5$, close to the numerical result $U_{c_1}/t \approx 12$ [7]. As N increases, the CSL becomes more robust with respect to U/t , in line with flatter Hofstadter band (Fig 1) that enhances correlation effects.

The critical theory between IQH and CSL—In this section, we establish the critical theory at the critical point between IQH phase and CSL phase. The effective field theory near the critical point can be described by two degrees of freedom: the charged rotor field ϕ and the spinon f_σ . This criticality can be understood in terms of holon condensation. To go beyond mean-field calculations an effective field theory for the critical point is constructed by minimally coupling the rotor field ϕ to the emergent gauge field a_μ , capturing the gauge fluctuations inherent to the rotor formalism. The effective theory can be written as[22]

$$\begin{aligned} \mathcal{L} &= \mathcal{L}[\phi, a, A, \lambda] + \mathcal{L}[\alpha, a] \\ \mathcal{L}[\phi, a, A, \lambda] &= \frac{1}{g} |(\partial_\mu - ia_\mu + iA_\mu)\phi|^2 + \frac{i\lambda}{g} (|\phi|^2 - 1) \\ \mathcal{L}[\alpha, a] &= -\frac{1}{4\pi} \sum_i (\alpha_i d\alpha_i + ad\alpha_i), \end{aligned} \quad (6)$$

where $g \sim U/t$ and ϕ is the scalar rotor field. α is the gauge field of the spinons and A_μ is the probe field of the U(1) fermion number conservation[23]. The λ field originates from the hard constraint $(|\phi|^2 - 1)$ satisfied by the rotor field and is treated as the Lagrange multiplier. The Chern-Simons term of $\alpha_i d\alpha_i$ originates from integrating the spinon Chern bands. Further integrating out α_i 's, we are left with the rotor degrees of freedom. Then we arrive at the critical theory for the phase transition between the CSL and IQH:

$$\mathcal{L} = \frac{1}{g} |(\partial_\mu - ia_\mu + iA_\mu)\phi|^2 + \frac{i\lambda}{g} (|\phi|^2 - 1) + \frac{N}{4\pi} ada + \dots, \quad (7)$$

where the \dots represent the Maxwell term in our effective action that are ignored later. IQH and CSL phase are separated by the critical point. In the IQH($\delta \equiv g_c^{-1} - g^{-1} < 0$) phase the rotors spontaneously condense, which leads to the Higgs phase. The emergent gauge a and the

external gauge field A are locked. The effective theory reads $\mathcal{L} = \frac{N}{4\pi} AdA$. Thus the system is in the IQH phase. While in the CSL($\delta > 0$) phase there is a charge gap. Then the rotor field can be integrated out, which leads to the effective theory: $\mathcal{L} = \frac{N}{4\pi} ada$.

The spinon gap remains open through the transition process. Thus the low energy physics is dominated by the critical boson described by the equation 7 near the phase transition point. In the following, we discuss the physical consequence of the critical theory which can be tested experimentally.

The experimental signature—The specific heat of the system receives the contributions of the critical boson and spinon separately. Since the spinon is gapped, in the low-energy regime the only contribution comes from the critical boson, known to behave as[24] $C_V \sim T^2$. The compressibility near the transition point can be determined by the Ioffe-Larkin rules[25, 26], which can be expressed as the contributions from the critical boson and the spinon $\kappa^{-1} = \kappa_b^{-1} + \kappa_f^{-1}$. We have $\kappa_b \sim T$, while $\kappa_f = 0$ since spinons are gapped. The critical theory is incompressible, although the charged rotors are gapless.

However, the transport properties near the critical point is more subtle. The resistivity obtained by the Chern-Simons RPA method[27] can be expressed as

$$\rho_e = \rho_\phi + \rho_f.$$

In our case, the ρ_ϕ and ρ_f are the resistivity tensors of the critical boson and spinon.

The spinon degrees of freedom form the Landau level, which leads to the anti-symmetric tensor ρ_f ,

$$\rho_f = \begin{pmatrix} 0 & \rho_H \\ -\rho_H & 0 \end{pmatrix}, \quad (8)$$

where $\rho_H = \frac{1}{N} \frac{h}{e^2}$. The spinon resistivity remains the same across the transition, as the spinon gap does not close. However, in the IQH phase, the holon condenses thus resistivity of holon $\rho_\phi = 0$ while in the CSL phase, $\rho_\phi = +\infty$. At the critical point the resistivity of the slave rotor is $\rho_\phi^c = R \frac{h}{e^2}$ and R can be evaluated numerically[28]. The resistivity for the critical rotors in Eq.(7), is a universal number intrinsic to the critical theory. Therefore, the total resistivity at the critical point should be:

$$\rho_e^c = \begin{pmatrix} R \frac{h}{e^2} & \rho_H \\ -\rho_H & R \frac{h}{e^2} \end{pmatrix}. \quad (9)$$

All the quantities R and ρ_H appearing in the above formula are the universal numbers. Combining the above arguments we expect the conductivity behaviors shown in Fig. 3 and predict there is a universal resistivity jump once the critical point is reached, which can be tested in transport measurements. The universal value R and dependence of the resistivity on the temperature and tuning

N	2	3	4	5	6	7	8
$\sigma_{xx}(e^2/h)$	0.87	1.02	1.08	1.11	1.12	1.14	1.15
$\sigma_{xy}(e^2/h)$	0.51	0.40	0.32	0.26	0.22	0.19	0.17

TABLE I. The longitudinal and transverse conductivities at the critical point for different N .

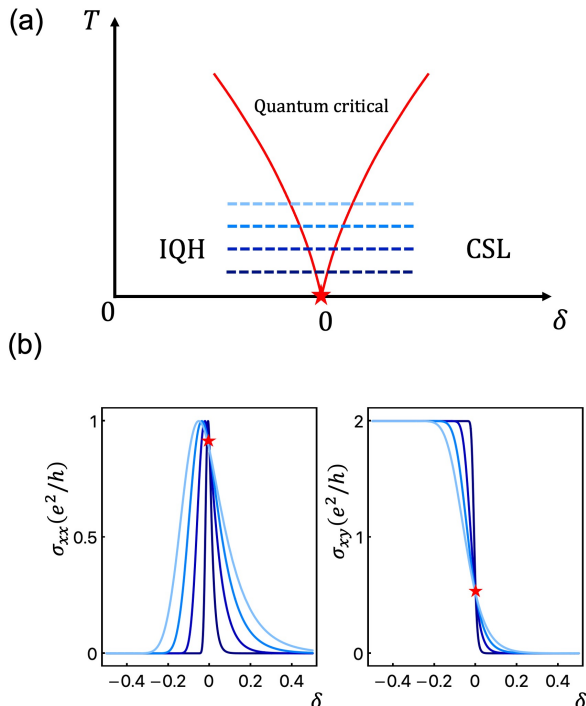


FIG. 3. (a) Schematic plot of the finite temperature phase diagram from the scaling theory (δ is the tuning parameter). The phase boundary (blue dotted line) between the quantum critical region and the topological phases is determined by $T = \delta^{\nu z}$. (b) The longitudinal (left) and transverse (right) conductivity when $N = 2$ by tuning the parameter δ at various temperatures. In the quantum critical fan, the conductivity curve is universal and can be obtained from quantum Boltzmann equation.

parameter can be calculated using the quantum Boltzmann equation[10, 28–32] from a large- N treatment:

$$\left(\frac{\partial}{\partial t} + s\mathbf{E} \frac{\partial}{\partial \mathbf{k}} \right) f_s(t, \mathbf{k}) = \frac{1}{2} I_\lambda(f_s(t, \mathbf{k})), \quad (10)$$

where $f_s(t, \mathbf{k})$ is the distribution function of the holon, $s = \pm 1$ and the right-hand side I_λ is the collision term. The details are explained in the Appendix and the critical conductivities are summarized in table I.

Conclusion and Discussion— We have demonstrated that the ground state of the Hofstadter-Hubbard model on the triangular lattice can host the integer quantum Hall fluid, chiral spin liquid, or VBS by employing the slave particle method. Additionally, we have deter-

mined the corresponding phase boundary at the mean-field level. By examining the critical theory, we find that there is a universal jump from the IQH to CSL phase transition. The universal conductivity intrinsic to the putative critical theory is obtained through quantum Boltzmann equation.

While we studied the continuous transition from IQH to CSL, it remains unknown about the nature of the transition from CSL to VBS. From parton mean-field employed in this paper, the magnetic phases is lacking. Therefore, future studies could employ advanced numerical techniques, such as density matrix renormalization group or quantum Monte Carlo simulations, to validate the phase diagram beyond mean-field approximations and diagnose the transition. Additionally, exploring doped regimes of the Hofstadter-Hubbard model may uncover correlated superconducting phases, as suggested by recent works[8].

Acknowledgments—XYS is grateful for related collaboration with Ashvin Vishwanath and Stefan Divic, and discussion with Subir Sachdev, Yong Baek Kim and Ya-Hui Zhang. Lu Zhang thanks Michael Hermele, Gang Chen, Xuping Yao and Ying Zhong for discussion on parton methods. Lu Zhang and RongNing Liu are supported by Early Career Scheme of Hong Kong Research Grant Council with grant No. 26309524 and startup fund at HKUST.

* songxy@ust.hk

- [1] P. W. Anderson, Resonating valence bonds: A new kind of insulator?, *Materials Research Bulletin* **8**, 153 (1973).
- [2] L. Savary and L. Balents, Quantum spin liquids: a review, *Reports on Progress in Physics* **80**, 016502 (2016).
- [3] S. R. White and A. Chernyshev, Néel order in square and triangular lattice heisenberg models, *Physical review letters* **99**, 127004 (2007).
- [4] D. A. Huse and V. Elser, Simple variational wave functions for two-dimensional heisenberg spin-1/2 antiferromagnets, *Physical review letters* **60**, 2531 (1988).
- [5] X. G. Wen, F. Wilczek, and A. Zee, Chiral spin states and superconductivity, *Phys. Rev. B* **39**, 11413 (1989).
- [6] R. B. Laughlin, Superconducting ground state of non-interacting particles obeying fractional statistics, *Phys. Rev. Lett.* **60**, 2677 (1988).
- [7] S. Divic, T. Soejima, V. Crépel, M. P. Zaletel, and A. Millis, Chiral spin liquid and quantum phase transition in the triangular lattice hofstadter-hubbard model, arXiv

- preprint arXiv:2406.15348 (2024).
- [8] S. Divic, V. Crépel, T. Soejima, X.-Y. Song, A. Millis, M. P. Zaletel, and A. Vishwanath, Anyon superconductivity from topological criticality in a hofstadter-hubbard model, arXiv preprint arXiv:2410.18175 (2024).
- [9] S. M. Chester, L. V. Iliesiu, M. Mezei, and S. S. Pufu, Monopole operators in u(1) chern-simons-matter theories, *Journal of High Energy Physics* **2018**, 1 (2018).
- [10] K. Damle and S. Sachdev, Nonzero-temperature transport near quantum critical points, *Physical Review B* **56**, 8714 (1997).
- [11] C. Kuhlenkamp, W. Kadow, A. Imamoğlu, and M. Knap, Chiral pseudospin liquids in moiré heterostructures, *Physical Review X* **14**, 021013 (2024).
- [12] J. Yang and X.-J. Liu, Chiral spin liquid phase in an optical lattice at mean-field level, *Physical Review B* **109**, 165108 (2024).
- [13] A. Heinz, A. J. Park, N. Šantić, J. Trautmann, S. Porsev, M. Safronova, I. Bloch, and S. Blatt, State-dependent optical lattices for the strontium optical qubit, *Physical review letters* **124**, 203201 (2020).
- [14] M. Aidelsburger, M. Atala, M. Lohse, J. T. Barreiro, B. Paredes, and I. Bloch, Realization of the hofstadter hamiltonian with ultracold atoms in optical lattices, *Physical review letters* **111**, 185301 (2013).
- [15] N. Cooper, J. Dalibard, and I. Spielman, Topological bands for ultracold atoms, *Reviews of modern physics* **91**, 015005 (2019).
- [16] J. K. Ding, L. Yang, W. O. Wang, Z. Zhu, C. Peng, P. Mai, E. W. Huang, B. Moritz, P. W. Phillips, B. E. Feldman, *et al.*, Particle-hole asymmetric ferromagnetism and spin textures in the triangular hubbard-hofstadter model, *Physical Review X* **14**, 041025 (2024).
- [17] C. Kuhlenkamp, *Aspects and probes of strongly correlated quantum phases in two dimensions*, Ph.D. thesis, Technische Universität München (2024).
- [18] G. Chen, K. R. Hazzard, A. M. Rey, and M. Hermele, Synthetic-gauge-field stabilization of the chiral-spin-liquid phase, *Physical Review A* **93**, 061601 (2016).
- [19] Y.-H. Zhang, D. Sheng, and A. Vishwanath, Su(4) chiral spin liquid, exciton supersolid, and electric detection in moiré bilayers, *Physical review letters* **127**, 247701 (2021).
- [20] X.-P. Yao, Y. Gao, and G. Chen, Topological chiral spin liquids and competing states in triangular lattice su(n) mott insulators, *Physical Review Research* **3**, 023138 (2021).
- [21] M. Hermele, V. Gurarie, and A. M. Rey, Mott insulators of ultracold fermionic alkaline earth atoms: Underconstrained magnetism and chiral spin liquid, *Physical Review Letters* **103**, 135301 (2009).
- [22] In Ref[8] the action of the critical mode is the complex ϕ^4 theory. The complex ϕ^4 and the O(2) non-linear sigma model describes the same universality class at the quantum critical point for dimensions $1 < d < 3$ [33].
- [23] In the following we neglect the response of the flavor degrees of freedom thus we do not include the spin gauge field A_s .
- [24] T. Senthil, Theory of a continuous mott transition in two dimensions, *Physical Review B—Condensed Matter and Materials Physics* **78**, 045109 (2008).
- [25] L. Ioffe and A. Larkin, Gapless fermions and gauge fields in dielectrics, *Physical Review B* **39**, 8988 (1989).
- [26] C. Chen, J.-X. Zhang, Z.-J. Song, and Z.-Y. Weng, Nonioffe-larkin composition rule and spinon-dictated electric transport in doped mott insulators, arXiv preprint arXiv:2406.15553 (2024).
- [27] S. H. Simon, The chern-simons fermi liquid description of fractional quantum hall states, in *Composite Fermions: A Unified View of the Quantum Hall Regime* (World Scientific, 1998) pp. 91–194.
- [28] W. Witczak-Krempa, P. Ghaemi, T. Senthil, and Y. B. Kim, Universal transport near a quantum critical mott transition in two dimensions, *Physical Review B—Condensed Matter and Materials Physics* **86**, 245102 (2012).
- [29] G. D. Mahan, *Many-particle physics* (Springer Science & Business Media, 2013).
- [30] S. Sachdev, Nonzero-temperature transport near fractional quantum hall critical points, *Physical Review B* **57**, 7157 (1998).
- [31] Y. Xu, X.-C. Wu, M. Ye, Z.-X. Luo, C.-M. Jian, and C. Xu, Interaction-driven metal-insulator transition with charge fractionalization, *Physical Review X* **12**, 021067 (2022).
- [32] P. Lee and X.-G. Wen, Quantum boltzmann equation of composite fermions interacting with a gauge field, *PHYSICAL REVIEW-SERIES B-* **52**, 17 (1995).
- [33] E. Brézin and J. Zinn-Justin, Spontaneous breakdown of continuous symmetries near two dimensions, *Physical Review B* **14**, 3110 (1976).

t-J model from the SU(N) Hofstadter-Hubbard model

In the large-U limit, each site is occupied by only one electron. The double occupancy will lead to the penalty of energy U . Thus we treat the Hubbard term $\sum_{j\alpha\neq\beta} n_{j\alpha}n_{j\beta}$ as the unperturbed term and perform the perturbation theory to the second order we obtain

$$H_2 = P_s \left[-\frac{t_{ij}t_{jk}}{U} \sum_{ijk} e^{-i(A_{ij}+A_{jk})} \left(\sum_{\alpha} c_{i\alpha}^{\dagger} c_{j\alpha} \right) \left(\sum_{\alpha\neq\beta} n_{j\alpha}n_{j\beta} \right) \left(\sum_{\alpha} c_{j\alpha}^{\dagger} c_{k\alpha} \right) \right] P_s, \quad (11)$$

where P_s is the projector that projects the many-body state to the single-occupied states. At half-filling, the kinetic term is annihilated, which gives rise to the usual spin-spin interaction $\sim S \cdot S$. The next order contribution is

$$H_3 = P_s \left[\sum_{ijkl} \frac{t_{ij} t_{jk} t_{kl}}{U^2} e^{-i(A_{ij} + A_{jk} + A_{kl})} \left(\sum_{\alpha} c_{i\alpha}^{\dagger} c_{j\alpha} \right) \left(\sum_{\alpha \neq \beta} n_{j\alpha} n_{j\beta} \right) \left(\sum_{\alpha} c_{j\alpha}^{\dagger} c_{k\alpha} \right) \left(\sum_{\alpha \neq \beta} n_{k\alpha} n_{k\beta} \right) \left(\sum_{\alpha} c_{k\alpha}^{\dagger} c_{l\alpha} \right) \right] P_s. \quad (12)$$

At half-filling, it is required that $i = l$, otherwise the term with $i \neq l$ creates a hole and double occupancy that vanishes under the projector P_s . This expression results in the chiral term. Now the effective Hamiltonian takes the form:

$$H = H_2 + H_3, \quad (13)$$

where H_2, H_3 read

$$H_2 = -\frac{2}{U} \sum_{\langle ij \rangle} t_{ij} t_{ji} c_{i\alpha}^{\dagger} c_{j\alpha} c_{j\beta}^{\dagger} c_{i\beta}, \quad (14)$$

$$H_3 = \frac{6}{U^2} \sum_{ijk \in \Delta} t_{ij} t_{jk} t_{ki} e^{-i\Phi_{\Delta}} c_{i\alpha}^{\dagger} c_{j\alpha} c_{j\beta}^{\dagger} c_{k\beta} c_{k\gamma}^{\dagger} c_{i\gamma},$$

where $\Phi_{\Delta} = A_{12} + A_{23} + A_{31}$ is the flux experienced by a single electron moving around a triangle. We assume hopping t_{ij} is not space-dependent $t_{ij} = t$. Thus the coupling $J_2 = \frac{2t^2}{U}$ and $J_3 = \frac{6t^3}{U^2}$. Expressing the above Hamiltonian in terms of the $SU(N)$ generators:

$$S_i^{\alpha\beta} = c_{i\alpha}^{\dagger} c_{i\beta}. \quad (15)$$

The Hamiltonian reads

$$H = J_2 \sum_{\langle ij \rangle} S_i^{\alpha\beta} S_j^{\beta\alpha} + J_3 \sum_{ijk \in \Delta} \exp(-i\Phi_{\Delta}) S_i^{\alpha\beta} S_j^{\beta\gamma} S_k^{\gamma\alpha}. \quad (16)$$

It is exactly the Hamiltonian (16) in the main body.

Details on solving the critical point of IQH/CSL transition

To solve the rotor Hamiltonian H_{θ} , we apply the imaginary time coherent path integral:

$$\mathcal{Z} = \int \mathcal{D}\psi^{\dagger} \mathcal{D}\psi \mathcal{D}\lambda \text{Exp} \left(- \int_{\tau} \sum_{\vec{k} \in \text{B.Z.}} \frac{1}{2U} |\partial_{\tau} \psi_{\vec{k}}|^2 - 2J\xi(\vec{k}) |\psi_{\vec{k}}|^2 - \int_{\tau} \lambda \sum_i (|\psi_i|^2 - 1) \right), \quad (17)$$

where λ is the Lagrangian multiplier for the constrain of unit field, $\vec{k} \in \text{B.Z.}$ refers to the summation conducting in the first Brillouin zone, and $\xi(\vec{k}) \equiv \cos k_x + \cos(\frac{k_x}{2} + \frac{\sqrt{3}}{2} k_y) + \cos(-\frac{k_x}{2} + \frac{\sqrt{3}}{2} k_y)$ describes the lattice configuration. The saddle point equation for λ can be obtained by integrating out the rotor field ψ :

$$\frac{1}{N_s} \sum_{\vec{k} \in \text{B.Z.}} \frac{U}{\omega_{\vec{k}}} = 1, \quad (18)$$

$\omega_{\vec{k}} = \sqrt{2U(\lambda - 2J\xi(\vec{k}))}$ is the band dispersion of rotor. When $\omega_{\vec{k}} = 0$, the rotor condenses and bounds with the spinon, indicating the IQH state. The critical point:

$$U_{c1} = 4J \left(\frac{1}{N_s} \sum_{\vec{k} \in \text{B.Z.}} \frac{1}{\sqrt{\xi(\vec{k})_{\text{max}} - \xi(\vec{k})}} \right)^{-2}. \quad (19)$$

By identifying the composition of rotor and spinon hopping $\langle \psi_i^\dagger \psi_j \rangle \langle f_i^\dagger f_j \rangle$ with the electron hopping $\langle c_i^\dagger c_j \rangle$, the parameter J can be estimated by combining the mean-field parameters \tilde{t} and J and the average energy of the lowest single particle electron band $\langle \epsilon_-(k) \rangle$:

$$J \approx \frac{|\langle \epsilon_-(k) \rangle| t}{z \tilde{t}}. \quad (20)$$

Using Fourier transformations, \tilde{t}/t can be approximated through the Green function of ψ (see Appendix A of [12]) :

$$\begin{aligned} \frac{\tilde{t}}{t} &= \frac{1}{z N_s} \sum_{\vec{k} \in \text{B.Z.}} 2\xi(\vec{k}) \frac{1}{\beta} \sum_n G_\psi(\vec{k}, \nu_n) \\ &= \frac{1}{z N_s} \sum_{\vec{k} \in \text{B.Z.}} \xi(\vec{k}) \frac{\sqrt{2U}}{\omega_{\vec{k}}} \\ &\stackrel{\text{C.P.}}{=} \sqrt{\frac{U_{c1}}{J}} \frac{1}{z N_s} \sum_{\vec{k} \in \text{B.Z.}} \frac{\xi(\vec{k})}{\sqrt{\xi(\vec{k})_{\text{max}} - \xi(\vec{k})}}. \end{aligned} \quad (21)$$

In a mean-field approach, all parameters are uniform in space and without complex phase factors. Combining Eq. 19, 20, 21 and substituting the values of $|\langle \epsilon_-(k) \rangle|$, we can easily obtain U_{c1} for different N in Fig. 2.

Quantum Boltzmann equation

In this section, we use the quantum Boltzmann equation to analyze the transport properties of the critical boson 7. We first generalize the action to the large- n case by introducing multiple flavors of the critical boson ϕ_α ,

$$\mathcal{L} = \frac{1}{g} \sum_{\alpha}^n |(\partial_\mu - ia_\mu + iA_\mu)\phi_\alpha|^2 + i\lambda(|\phi_\alpha|^2 - 1) + \frac{N}{4\pi} ada, \quad (22)$$

where the constraint $\sum_{\alpha=1}^n |\phi_\alpha|^2 = 1$ is imposed. When $n = 1$ the model reduces to the complex scalar field discussed in the main text. We consider the case where the external gauge field A_μ only couples with the $\alpha = 1$ component. The effective action of λ by integrating the rotor field out is

$$S_{\text{eff}}[\lambda] = n \left[\text{tr} \ln (-\partial^2 + i\lambda) - \frac{i}{g} \int \lambda \right]. \quad (23)$$

The λ field can be viewed as the mass m of the rotor field ϕ . By minimizing the effective action we can obtain the relation between the mass of the rotor and the coupling strength at a finite temperature:

$$\frac{m}{T} = \frac{1}{2} \sinh^{-1} \left(\frac{1}{2} e^{2\pi \frac{\delta}{T}} \right) \quad (24)$$

where δ is defined as $g_c^{-1} - g^{-1}$. From the above equation $\frac{m}{T} \approx 0.96$ at the critical point $\delta = 0$.

We express the boson field ϕ_1 as the composition of the creation and the annihilation operator:

$$\phi_1(\mathbf{x}, t) = \int_{\mathbf{k}} b_-(\mathbf{k}, t) e^{i\mathbf{k} \cdot \mathbf{x}} + b_+^\dagger(\mathbf{k}, t) e^{-i\mathbf{k} \cdot \mathbf{x}}. \quad (25)$$

We define the distribution function to be

$$f_s(t, \mathbf{k}) = \langle b_s^\dagger(t, \mathbf{k}) b_s(t, \mathbf{k}) \rangle, \quad (26)$$

where s denotes $+$, $-$. The quantum Boltzmann equation of the distribution function reads

$$\left(\frac{\partial}{\partial t} + s \mathbf{E} \cdot \frac{\partial}{\partial \mathbf{k}} \right) f_s(t, \mathbf{k}) = \frac{1}{2n} I_\lambda(f_\pm(t, \mathbf{k})), \quad (27)$$

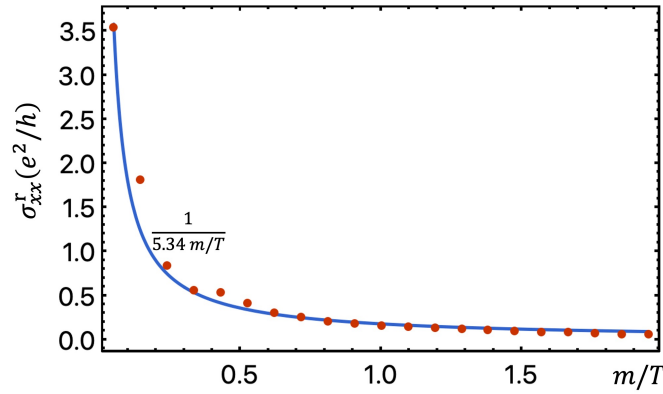


FIG. 4. Rotor conductivity versus the rotor mass m over temperature T . The red dotted line is the value calculated numerically while the blue line is the function that fit the calculated value.

where I_λ are the collision terms that can be defined as

$$\begin{aligned}
 I_\lambda(f_\pm) = & \int_0^\infty \frac{d\Omega}{\pi} \int \frac{d^2\mathbf{q}}{(2\pi)^2} \text{Im}(D_\lambda(\mathbf{q}, \Omega)) \times \\
 & \left\{ \frac{2\pi\delta(\epsilon_{\mathbf{k}} - \epsilon_{\mathbf{k}+\mathbf{q}} + \Omega)}{4\epsilon_{\mathbf{k}}\epsilon_{\mathbf{k}+\mathbf{q}}} (f_s(t, \mathbf{k}) [1 + f_s(t, \mathbf{k} + \mathbf{q})] n_{\mathbf{q}}(\Omega) - [1 + f_s(t, \mathbf{k})] f_s(t, \mathbf{k} + \mathbf{q}) [1 + n_{\mathbf{q}}(\Omega)]) \right. \\
 & \frac{2\pi\delta(\epsilon_{\mathbf{k}} - \epsilon_{\mathbf{k}+\mathbf{q}} - \Omega)}{4\epsilon_{\mathbf{k}}\epsilon_{\mathbf{k}+\mathbf{q}}} (f_s(t, \mathbf{k}) [1 + f_s(t, \mathbf{k} + \mathbf{q})] [1 + n_{\mathbf{q}}(\Omega)] - [1 + f_s(t, \mathbf{k})] f_s(t, \mathbf{k} + \mathbf{q}) n_{\mathbf{q}}(\Omega)) \\
 & \left. \frac{2\pi\delta(\epsilon_{\mathbf{k}} + \epsilon_{-\mathbf{k}+\mathbf{q}} - \Omega)}{4\epsilon_{\mathbf{k}}\epsilon_{-\mathbf{k}+\mathbf{q}}} (f_s(t, \mathbf{k}) f_{-s}(t, -\mathbf{k} + \mathbf{q}) [1 + n_{\mathbf{q}}(\Omega)] - [1 + f_s(t, \mathbf{k})] [1 + f_{-s}(t, -\mathbf{k} + \mathbf{q})] n_{\mathbf{q}}(\Omega)) \right\}. \quad (28)
 \end{aligned}$$

Here assume that the boson of the order parameter is in the equilibrium. Thus we approximate the distribution of the boson as Bose-Einstein distribution $n_{\mathbf{q}}(\Omega) = 1/(e^{\beta\Omega} - 1)$. The propagator of the λ field D_λ is

$$D_\lambda^{-1}(\mathbf{q}, i\Omega_n) = T \sum_m \int_{\mathbf{k}} \frac{1}{(\nu_m + \Omega_n)^2 + \epsilon_{\mathbf{k}+\mathbf{q}}^2} \frac{1}{\nu_m^2 + \epsilon_{\mathbf{k}}^2}, \quad (29)$$

where $\epsilon_{\mathbf{k}}$ is the dispersion of the ϕ field and $i\Omega_n$ implies the Matsubara frequency. The real frequency result is obtained by the analytical continuation to the real value. Then the above equation can be linearized and solved by linear algebra approach. We obtain the rotor conductivity shown in Fig. 4.

Since the convergency of the numerical integral of the quantum Boltzmann equation suffers when m/T becomes small it is more computationally economical to use the function $\frac{1}{\alpha(m/T)}$ to extrapolate the function. The α is used to fit the function and it is chosen to be 5.34. The choice of the function is physically reasonable in the limit $m/T \rightarrow 0$ and $m/T \rightarrow \infty$. In these two cases, the rotor conductivities are expected to be ∞ and 0. Therefore, it is sufficient to capture the low-temperature physics using the approximate function. While the conductivity at the critical point is determined accurately without approximation.